MEASUREMENT SCIENCE REVIEW

Evaluation of Absorbing Material Shielding Effectiveness Using a Baum–Liu–Tesche Based Method

Chunmei Dou[1], Rumeng Wang [2], Hsiung-Cheng Lin[3*] , Yan Zhang[2], Jiayi Chai[2]

[1]*Sifang College, Shijiazhuang Tiedao University, No. 1, Jia Zhuangyuan Road, 051132, Shijiazhuang, China,*
568880437@qq.com
[2]*School of Electrical Engineering, Hebei University of Science and Technology, No. 26, Yuxiang Street, 050018,*
Shijiazhuang, China, 2841034951@qq.com, yanyanfly163@163.com, 2674398101@qq.com
[3]*Department of Electronic Engineering, National Chin-Yi University of Technology, No.57, Sec. 2, Zhongshan Road,*
Taiping Dist., 411030, Taichung, Taiwan, hclin@ncut.edu.tw

Abstract: The shielding efficacy of the metal cavity can be effectively enhanced using absorbing materials coated on the inner wall of the cavity. With highly potential materials such as graphene, silicon carbide (SiC), polytetrafluoroethylene (PTFE), and Ni/rGO in shielding, an analytical method based on the Baum–Liu–Tesche (BLT) equation is proposed to evaluate their shielding effectiveness (SE) in the open cavity. Compared to the electromagnetic field simulation software, i.e., CST Studio Suite, the resonant frequency of the coated cavity using the proposed model can be obtained with an average error of no more than 8 dB. The findings reveal that PTFE with a 1 mm thickness coated on the inner wall of the cavity can achieve the best shielding effect, but the resonant frequency of the cavity remains unchanged. On the other hand, the increased material thickness by adding the other three materials has no effect on the frequency located at the resonance modes of TE101 and TE102, except for the high-order resonance TE103. However, it is found that when a 2 mm thickness of these three materials is coated, the shielding ability achieves its best status. It verifies that the proposed BLT analytical method presents superiority in terms of computational rapidity and accuracy, with fewer resources occupied.

Keywords: shielding effectiveness, BLT equation, absorbing material, cavity shielding, electromagnetic shielding

1. INTRODUCTION

With the rapid development of electronic technology, the degree of integration and miniaturization in electronic devices are constantly improving. As a result, the problem of the space electromagnetic environment is getting more attention [1]-[2]. For this issue, the shielding cavity is often used to carry out electromagnetic shielding. Typically, different shaped holes are used for heat dissipation to reduce electromagnetic interference within the shielding cavity. However, the existence of holes creates a coupling channel that disturbs electromagnetic wave propagation, resulting in a sharp weakening of the shielding ability of the cavity [3].

At present, some analytical methods, such as the Bethe small-hole coupling [4], the Robinson equivalent circuit [5], and the Baum–Liu–Tesche (BLT) equation [6], offer the advantage of high calculation efficiency with fewer resources demanded in the shielding effectiveness (SE) calculation of the coated porous cavity [7]. However, the field distribution in the cavity must be calculated from the electromagnetic field, making the computational process more complicated. Based on the transmission line theory, an equivalent circuit

model was established to determine electromagnetic SE of metal cavities covered with medium conductivity materials [8]. The position and resonance effect on SE were calculated and analyzed in this work. Alternatively, an analytical model for SE evaluation in irregular cavities under plane wave irradiation was developed using coupled electromagnetic topology theory and the BLT equation [9]. The factors affecting the SE of cavities were explored. Nevertheless, the study on the analysis of inner coating materials in the shielding cavity is still limited in this field.

The mainstream absorbing materials coated on the inner wall of the shielding cavity mainly include graphene, silicon carbide (SiC), polytetrafluoroethylene (PTFE), and Ni/rGO composites. Graphene offers advantages such as low density, corrosion resistance, good thermal stability, high conductivity, and a simple process, making it a new type of effective electromagnetic shielding or microwave absorption material [10]. SiC has strong radiation resistance, high working intensity, high thermal conductivity, good oxidation resistance, and good chemical corrosion resistance [11]. PTFE is a high-performance coating with good corrosion

Corresponding author: hclin@ncut.edu.tw (H.C. Lin)

resistance, temperature resistance, wear resistance, and aging resistance [12]. On the other hand, Ni/rGO composite is an electromagnetic wave absorption material that combines Ni nanoparticles with graphene [13]. As mentioned above, graphene, SiC, PTFE, and Ni/rGO are considered potential shielding materials to be studied in this research.

2. PRINCIPLE OF ELECTROMAGNETIC SHIELDING IN WAVE-ABSORBING MATERIAL

Due to the impedance mismatch between the absorbing material and the surrounding free space, the coupling of the electromagnetic energy can be absorbed and dissipated through conversion of heat into power when the electromagnetic wave enters the absorbing material [13]. To achieve effective absorption, two conditions must be satisfied:

i. When an incident electromagnetic wave enters the absorbing material from a free space, most of the wave must enter the interior of the material rather than reflect back.

ii. Electromagnetic waves entering the material must be effectively converted into thermal energy for power dissipation.

By employing conductive or magnetic materials to construct a shielding enclosure, electromagnetic isolation can be achieved in a specific area. It means that the electromagnetic fields inside the area can be contained without leakage, while external radiating electromagnetic fields are blocked from penetration. Maxwell's equations provide the fundamental theoretical basis for addressing electromagnetic compatibility issues, formulating the intrinsic relationships between electric fields, magnetic fields, current density, and charge density. Indeed, electromagnetic waves are dynamic manifestations of electromagnetic fields, representing periodically varying electromagnetic fields propagating through space. The oscillation directions of the electric and magnetic fields are mutually perpendicular and orthogonal to the direction of wave propagation. The expressions for electric field strength E_x and magnetic field strength H_y are expressed as follows [14]:

$$E_x(t,z) = E_{xm} \cos (\omega t - kz)e_x \tag{1}$$

$$H_y(t,z) = H_{ym} \cos (\omega t - kz)e_y = \frac{kE_{xm}}{\mu\omega}(\omega t - kz)e_y \tag{2}$$

where the electromagnetic wave propagates along the negative z-axis direction. E_{xm} is the amplitude of the electric field in the x-axis direction, H_{ym} is the amplitude of the magnetic field in the y-axis direction, t represents time, ω is the angular frequency of the electromagnetic wave, and $k = \omega\sqrt{\mu\varepsilon}$ is the wavenumber, which denotes the phase change per unit distance of electromagnetic waves. In free space, the wavenumber k is given by $k_1 = \omega\sqrt{\mu_0\varepsilon_0}$, μ_0 is the relative permeability in free space, ε_0 is the relative permittivity of free space, and k_1 is a real number. When electromagnetic waves propagate into the cavity and are absorbed by the absorbing material, the wavenumber k is

given by $k_r = \omega\sqrt{\mu_r\varepsilon_r}$, where ε_r is the relative permittivity of the absorbing material, and μ_r is the relative permeability of the absorbing material [15].

Combined with the law of conservation of electromagnetic field energy [16], it is deduced as

$$\begin{cases} w_e = w_m, \ \boldsymbol{D} = \varepsilon\boldsymbol{E}, \ \boldsymbol{B} = \mu\boldsymbol{H} \\[2mm] w_e = \frac{1}{2}\boldsymbol{E} \cdot \boldsymbol{D} = \frac{1}{2}\varepsilon|\boldsymbol{E}|^2 \\[2mm] w_m = \frac{1}{2}\boldsymbol{H} \cdot \boldsymbol{B} = \frac{1}{2}\mu|\boldsymbol{H}|^2 \end{cases} \tag{3}$$

where w_e and w_m represent the electric field energy density and magnetic field energy density, respectively. $\boldsymbol{E}$ denotes the electric field intensity, $\boldsymbol{H}$ denotes the magnetic field intensity, $\boldsymbol{D}$ is the electric displacement vector, $\boldsymbol{B}$ is the magnetic flux density, ε is the permittivity, and μ is the permeability.

When an electromagnetic wave propagates through free space and impinges on the interface of another medium, the free space impedance Z_0 is obtained from (3), as shown (4). The surface impedance Z_S of the wave-absorbing material is given by (5) [17]:

$$Z_0 = \frac{|\boldsymbol{E}|}{|\boldsymbol{H}|} = \sqrt{\frac{\mu_0}{\varepsilon_0}} \tag{4}$$

$$Z_S = Z_m \cdot \tan(\gamma_m \cdot d_m) \tag{5}$$

where $Z_m = \sqrt{\mu_r/\varepsilon_r}$ is the intrinsic impedance of the wave-absorbing material, $\gamma_m = j\omega\sqrt{\mu_r\varepsilon_r}$ is the propagation constant of the wave-absorbing material, and d_m is the thickness of the wave-absorbing coating layer. One portion of the wave is reflected back, while the other portion enters the material. Through the combined effects of dielectric loss and magnetic loss, the absorbing material converts the electromagnetic wave into thermal energy or other forms of energy, thereby attenuating the electromagnetic wave.

The BLT equation can describe the equivalent transmission characteristics of electromagnetic waves on transmission lines, including the propagation and absorption properties when electromagnetic waves enter the cavity interior. When establishing this model, the external electric field strength is converted into an equivalent potential (voltage) based on the principle of field-circuit equivalence. If an external electro-magnetic wave irradiates the cavity aperture, the tangential electric field component $\boldsymbol{E}_{\tan}^{inc}(z)$ across the aperture serves as the key field variable. By introducing the effective aperture height h_{eff}, the tangential electric field is directly equivalent to a distributed voltage source $\boldsymbol{V}_s(z)$ on the transmission line [18]:

$$\boldsymbol{V}_s(z) = \boldsymbol{E}_{\tan}^{inc}(z) \cdot h_{eff} \tag{6}$$

To match the wave modes of the transmission line, a mode-matching integration is performed on this distributed source, yielding lumped equivalent wave sources V_0^+ and V_0^- that can be injected into the BLT equation network model [19]:

$$V_0^{\pm} = \frac{1}{2} \int \boldsymbol{V}_s(z) e^{\mp j\beta z} \, \mathrm{d}z \qquad (7)$$

The voltage values at each node of the network are then obtained, completing the analysis of the shielding characteristics of the cavity. Based on the aforementioned electromagnetic energy flow relationships, the signal flow graph of the cavity model constructed is shown in Fig. 1. It demonstrates the transmission paths and energy conversion processes of electromagnetic waves within the cavity structure.
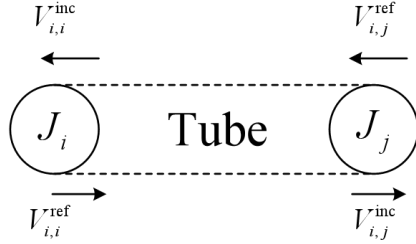
Fig. 1. Signal flow diagram of cavity model.

Here $\boldsymbol{V}_{i,i}^{\mathrm{inc}}$ and $\boldsymbol{V}_{i,i}^{\mathrm{ref}}$ represent the incident and reflected voltages, respectively, at node J_i on the transmission channel Tube; $\boldsymbol{V}_{i,j}^{\mathrm{inc}}$ and $\boldsymbol{V}_{i,j}^{\mathrm{ref}}$ represent the incident and reflected voltages, respectively, at node J_j on the transmission channel Tube. According to Fig. 1, the transmission equation, scattering equation, and voltage equation are expressed in (8), (9) and (10), respectively. As a result, the BLT equation can be obtained in (10) [13].

$$\boldsymbol{V}_{i,j}^{\mathrm{ref}} = \boldsymbol{P}\,\boldsymbol{V}_{i,j}^{\mathrm{inc}} - \boldsymbol{V} \qquad (8)$$

$$\boldsymbol{V}_{i,j}^{\mathrm{ref}} = \boldsymbol{S}\,\boldsymbol{V}_{i,j}^{\mathrm{inc}} \qquad (9)$$

$$\boldsymbol{V}_{i,j} = \boldsymbol{V}_{i,j}^{\mathrm{inc}} + \boldsymbol{V}_{i,j}^{\mathrm{ref}} \qquad (10)$$

$$\boldsymbol{V}_{i,j} = (\boldsymbol{S} + \boldsymbol{E})\,(\boldsymbol{P} - \boldsymbol{S})^{-1}\,\boldsymbol{V} \qquad (11)$$

where $\boldsymbol{V}_{i,j}$ represents the total voltage vector of the node; $\boldsymbol{S}$ represents the node scattering matrix, $\boldsymbol{E}$ represents the identity matrix; $\boldsymbol{P}$ represents the transmission matrix of the transmission channel, $\boldsymbol{V}$ represents the equivalent voltage source vector of the node, the unit vector composed of an equivalent voltage source V_0, i.e. $\boldsymbol{V} = [V_0\ 0\ 0\ 0\ldots 0]^T$.

3. BLT-based equation model

Results should be briefly summarized, and the authors' main scientific contributions should be demonstrated.

In this study, the rectangular open-hole shielding cavity is taken as an example for SE analysis, and its schematic diagram is shown in Fig. 2. Here, absorbing materials are selected based on their electromagnetic parameters, such as the relative dielectric constant ε_r and relative magnetic permeability μ_r [13]. The rectangular hole gap has length l_1

and width w_1, located in the center of the front wall in the cavity. The direction of the interference electromagnetic wave electric field is along the y axis, and the propagation direction is along the $-z$ axis, that is, vertical incidence and vertical polarization. The distance between the observation point P$_2$ and the aperture center is d_2. The distance between the observation point P$_1$ and the aperture center is d_1; the SE of the rectangular shielding cavity is obtained by calculating the voltage at the observation point P$_1$.
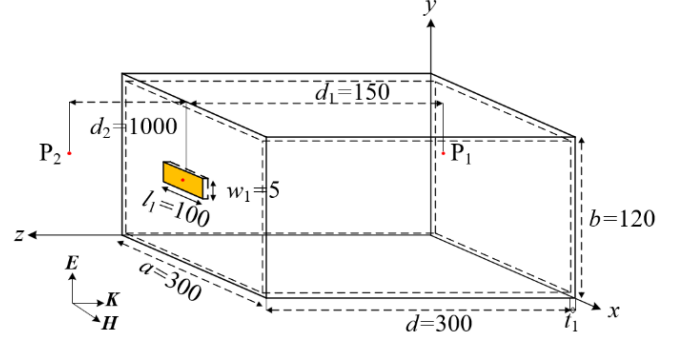

Fig. 2. Schematic diagram of rectangular cavity model structure (unit: mm).

The schematic diagram of a cavity coated with and without absorbing material is shown in Fig. 3, where the gray area indicates no absorbing material coated, and the blue area shows the inner wall of the cavity coated with absorbing material.
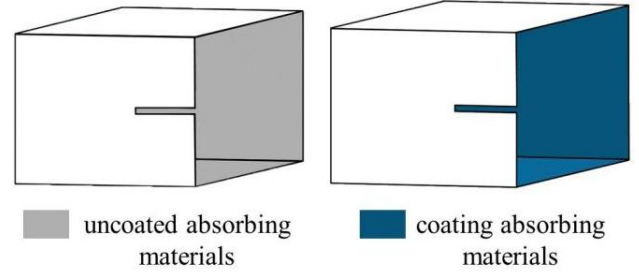

Fig. 3. Coating schematic diagram in rectangular shielding cavities with openings.

When coating absorbing materials on the inner wall of the cavity and establishing the equivalent circuit, the aperture impedance is equivalent to Z_{ap}, which can be expressed as the parallel connection of Z_{ap1} and Z_{ap2}. The equivalent impedance of the aperture is Z_{ap1} ($Z_{\mathrm{ap1}} = 1/Y_{\mathrm{ap1}}$). When using coated absorbing materials, the equivalent impedance of the absorbing material at the aperture is Z_{ap2} ($Z_{\mathrm{ap2}} = 1/Y_{\mathrm{ap2}}$). Z_{gmn1} is the characteristic impedance of the rectangular cavity, and Z_{gmn2} is the characteristic impedance of the coated absorbing material waveguide. The impedance at the inner wall of the rectangular cavity is equivalent to the parallel connection of Z_{gmn1} and Z_{gmn2}. The equivalent circuit of anti-interference using the coating material against electromagnetic wave irradiation is therefore established, as shown in Fig. 4.
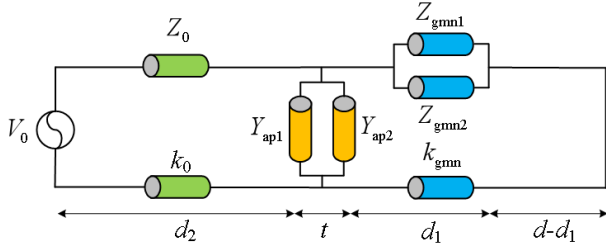
Fig. 4. Equivalent circuit of cavity inner wall.

According to the transmission line equivalent circuit [20], voltage source V_0 ($V_0 = 1$ V) represents the external incident plane wave, and Z_0 ($Z_0 = 377$ Ω) is the characteristic impedance of free space; the external space transmission coefficient $k_0 = 2\pi/\lambda$, where λ is the interference electromagnetic wavelength.

The equivalent impedance Z_{ap1} of the aperture is expressed as

$$Z_{ap1} = j \frac{1}{2} \frac{l_1}{a} Z_{os} \tan\left(\frac{k_0 l_1}{2}\right) \tag{12}$$

where Z_{os} is the equivalent impedance of the perforated cavity wall.

Z_{os} is expressed as

$$Z_{os} = 120\pi^2 \left[\ln\left(2 \frac{1 + \sqrt[4]{1 - (w_e/b)^2}}{1 - \sqrt[4]{1 - (w_e/b)^2}}\right)\right]^{-1} \tag{13}$$

where w_e is the effective width of the coplanar transmission line, and $w_e = l_1 - (5t/4\pi)[1 + \ln(4\pi l_1/t)]$. The transmission coefficient k_g of the cavity coated with absorbing materials is $2\pi (\varepsilon_r \mu_r)^{1/2}/\lambda$. The wall impedance Z_{ap2} in the cavity is used to characterize the absorption capability against an incident electromagnetic wave, expressed in (14).

$$Z_{ap2} = \left[\ln\left(2 \frac{1 + \sqrt[4]{1 - (w_e/b)^2}}{1 - \sqrt[4]{1 - (w_e/b)^2}}\right)\right]^{-1} \cdot \frac{j120\pi^2 l_1 \tan\left(\frac{\pi l_1}{\lambda} \sqrt{\varepsilon_r \mu_r}\right)}{2a} \tag{14}$$

where ε_r and μ_r represent the relative dielectric constant and relative permeability of the absorbing material filled with the cavity, respectively. Note that the influence of the hole seam position on the impedance of the hole array is ignored.

The impedance and transmission coefficients in the shielding cavity are equivalent to Z_{gmn1} and k_{gmn1} in the rectangular waveguide, respectively.

$$Z_{gmn1} = Z_0 / \sqrt{1 - \left(\frac{m\lambda}{2a}\right)^2 - \left(\frac{n\lambda}{2b}\right)^2} \tag{15}$$

$$k_{gmn1} = k_0 \sqrt{1 - \left(\frac{m\lambda}{2a}\right)^2 - \left(\frac{n\lambda}{2b}\right)^2} \tag{16}$$

In (15) and (16), the values of m and n are the number of standing waves along the x and y axes. The characteristic impedance Z_{gmn2} of a waveguide coated with absorbing material is expressed as

$$Z_{gmn2} = \frac{2d}{a} \cdot \frac{Z_0}{\sqrt{1 - (f_c/f)^2}} \cdot \frac{k_1}{\gamma} \tag{17}$$

where a and d are the length and width dimensions of the cavity in the model shown in Fig. 2, respectively, and $f_c = c/2d$ is the cutoff frequency of the dominant mode (TE_{10}) of the rectangular waveguide [13], with c as the speed of light in vacuum and as the operating frequency γ is the complex propagation constant of the rectangular waveguide after coating with absorbing material. This is due to the introduction of the complex impedance boundary condition resulting from the inner walls coated with absorbing material. The complex propagation constant γ must be determined by solving the eigenvalue equation. When the material loss is relatively small, the perturbation method can be adopted for efficient solution [15], and the expression of γ can be derived as shown in (18).

$$\gamma = \sqrt{k_c^2 - k_1^2 + j \frac{2k_1}{aZ_0} \cdot Z_S} = \alpha - j\beta \tag{18}$$

where $k_c = \pi/d$ is the cutoff wavenumber, α and β are the real and imaginary parts of γ, respectively [21]. Substituting (17) into (18) yields (19).

$$Z_{gmn2} = \frac{2d}{a} \cdot \frac{Z_0}{\sqrt{1 - (f_c/f)^2}} \cdot \frac{k_1}{\alpha - j\beta} \tag{19}$$

The equivalent impedance Z_{ap} of the slot in Fig. 4 is shown in (20), and the total impedance Z_{gmn} of the rectangular waveguide is shown in (21).

$$Z_{ap} = Z_{ap1}//Z_{ap2} =$$

$$= \left[\ln\left(2 \frac{1 + \sqrt[4]{1 - (w_e/b)^2}}{1 - \sqrt[4]{1 - (w_e/b)^2}}\right)\right]^{-1} \cdot \frac{j3\pi^2 l_1}{a} \cdot \frac{\tan\left(\frac{\pi l_1}{\lambda}\right) \tan\left(\frac{\pi l_1}{\lambda} \sqrt{\frac{\varepsilon_r}{\mu_r}}\right)}{\tan\left(\frac{\pi l_1}{\lambda}\right) + \tan\left(\frac{\pi l_1}{\lambda} \sqrt{\frac{\varepsilon_r}{\mu_r}}\right)} \tag{20}$$

$$Z_{gmn} = Z_{gmn1}//Z_{gmn2} =$$

$$= \frac{d\lambda Z_0^2}{a(\alpha - j\beta)\sqrt{1 - \left(\frac{f_c}{f}\right)^2} + d\lambda Z_0 \sqrt{1 - \left(\frac{m\lambda}{2a}\right)^2 - \left(\frac{n\lambda}{2b}\right)^2}} \tag{21}$$

According to the electromagnetic topology theory [17], the signal flow diagram of the cavity using the coated suction material is established as shown in Fig. 5. Here, Tube1 represents free space, and Tube2 and Tube3 are shielded

cavity, where J_1 is the cavity in vitro observation point P_2, W_s is the interference electromagnetic wave equivalent voltage source, J_2 is the hole seam node, J_3 is the intra-cavity observation point P_1, and J_4 is the terminal node of the cavity.
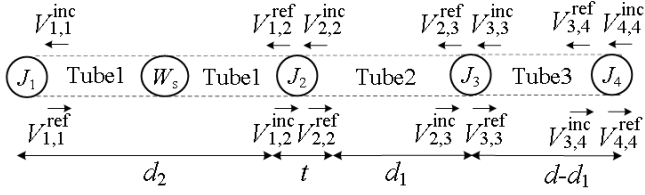

Fig. 5. Signal-flow graph of cavity coated with absorbing material.

The BLT equation, formed from the inner wall using a coated absorbing material cavity, is established based on Fig. 4 and Fig. 5. The scattering matrix S can be obtained from the impedance, $S = diag\ [\rho_1\rho_2\rho_3\rho_4]$. ρ_1 indicates the node J_1 dissipation coefficient, and $\rho_1 = 0$, ρ_4 is the node J_4 dissipation coefficient, and $\rho_4 = -1$. $\rho_i\ (i = 2,3,4)$ represents the node J_j of the scattering matrix, expressed by (22).

$$\begin{cases} \rho_2 = \begin{bmatrix} \dfrac{Y_0 - Y_{gmn} - Y_{ap}}{Y_0 + Y_{gmn} + Y_{ap}} & \dfrac{2Y_{gmn}}{Y_0 + Y_{gmn} + Y_{ap}} \\ \dfrac{2Y_0}{Y_0 + Y_{gmn} + Y_{ap}} & \dfrac{Y_{gmn} - Y_{ap} - Y_0}{Y_0 + Y_{gmn} + Y_{ap}} \end{bmatrix} \\ \\ \rho_3 = \begin{bmatrix} 0 & 1 \\ 1 & 0 \end{bmatrix} \end{cases} \quad (22)$$

where $Y_0(= 1/Z_0)$ represents the free space admittance, and $Y_{gmn}(= 1/Z_{gmn})$ represents a rectangular waveguide guide.

The transmission coefficient comprises the free-space transmission coefficient k_0 and the transmission coefficient k_g after the cavity is coated with an absorbing material. The transmission matrix P can be derived from the transmission coefficient, $P = diag\ [T_1T_2T_3]$, where $T_i\ (i = 1,2,3)$ is the transmission matrix of each segment transmission channel, as expressed in (23).

$$\begin{cases} T_1 = \begin{bmatrix} 0 & e^{ik_0d_2} \\ e^{ik_0d_2} & 0 \end{bmatrix} \\ \\ T_2 = \begin{bmatrix} 0 & e^{ik_gd_1} \\ e^{ik_gd_1} & 0 \end{bmatrix} \\ \\ T_3 = \begin{bmatrix} 0 & e^{ik_g(d-d_1)} \\ e^{ik_g(d-d_1)} & 0 \end{bmatrix} \end{cases} \quad (23)$$

Substitute the scattering matrix S (19) and the transmission matrix P (20) into (10) to obtain the total voltage $V_{3,3}$ at observation point P_1, and thus obtain the SE of the cavity, as shown in (24).

$$SE = 20\lg\ (V_0/V_{3,3}) \quad (24)$$

Therefore, the basic process flow diagram of the BLT equation modeling principle for the SE of the cavity coated with absorbing materials on the inner wall is shown in Fig. 6.
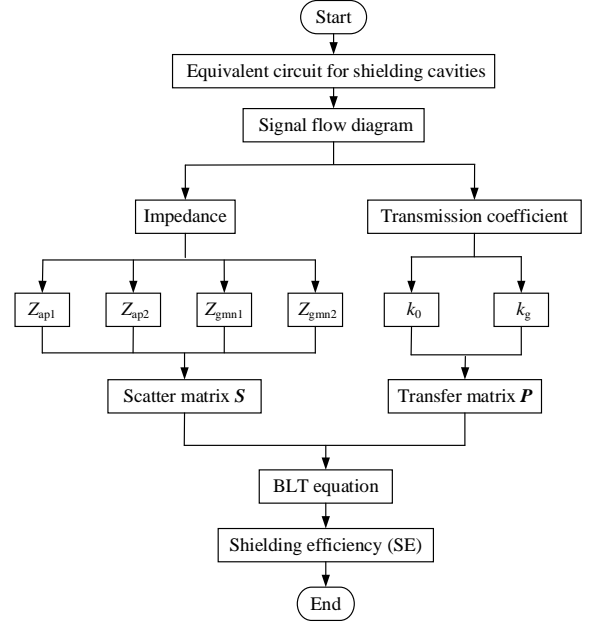

Fig. 6. Flowchart of BLT equation modeling.

4. MODEL VERIFICATION AND ANALYSIS

A. *Model verification*

Taking the shielding cavity model shown in Fig. 2 as an example, this paper examines the effectiveness of the BLT equation topology using four absorbing materials: graphene [20], SiC [22], PTFE, and Ni/rGO composite materials [23]. The electromagnetic parameters of the absorbing material are shown in Table 1.

Table 1. Electromagnetic parameters in absorbing materials.

Material	Relative permittivity ε_r	Relative permeability μ_r
Graphene	4.5	1.01
SiC	4.1	0.64
PTFE	2.01	0.95
Ni/rGO	13.45	1.14

The cavity resonance frequency f_{mnp} is derived from the wave equation. The cavity resonance frequency is expressed in (25)

$$f_{mnp} = \frac{c}{2\pi\sqrt{\varepsilon_r\mu_r}}\sqrt{\left(\frac{m\pi}{a}\right)^2 + \left(\frac{n\pi}{b}\right)^2 + \left(\frac{p\pi}{d}\right)^2} \quad (25)$$

where c is the speed of light, ε_r is the dielectric constant, and μ_r is the relative permittivity [15]. m, n and, p are the number of standing waves along the x, y, and z axes, respectively. A resonant frequency f_{mnp} corresponds to a resonant mode TE_{mnp}. When m and n in the resonant mode TE_{mnp} are taken as 1 and 0, respectively, the resonant mode TE_{10p} is regarded as the resonant primary mode, where the weakest SE arises [24].

Set the frequency step $\Delta f = 0.001$ GHz at a range of 0-2 GHz with 2000 sampling points q. The calculation results from the BLT equation and CST are depicted as r_{BLT} and r_{CST}, respectively. The error (Δ) between r_{BLT} and r_{CST} is defined in (26). The average error ($\overline{\Delta}$) between the BLT equation and the CST simulation is shown in (27).

$$\Delta = |r_{BLT} - r_{CST}| \tag{26}$$

$$\overline{\Delta} = \frac{\sum_{q=1}^{2000}|\Delta|}{2000} \tag{27}$$

The hardware system used to implement the proposed model and CST software was an Intel i5-1135G7 2.4 GHz CPU and 16 GB memory workstation. Among four different materials, the comparison of SE vs frequency between the BLT equation and CST is shown in Fig. 7. The error (Δ) curve is shown in Fig. 8.

(a) SE comparison between BLT and CST with PTFE

(b) SE comparison between BLT and CST with SiC

(c) SE comparison between BLT and CST with graphene

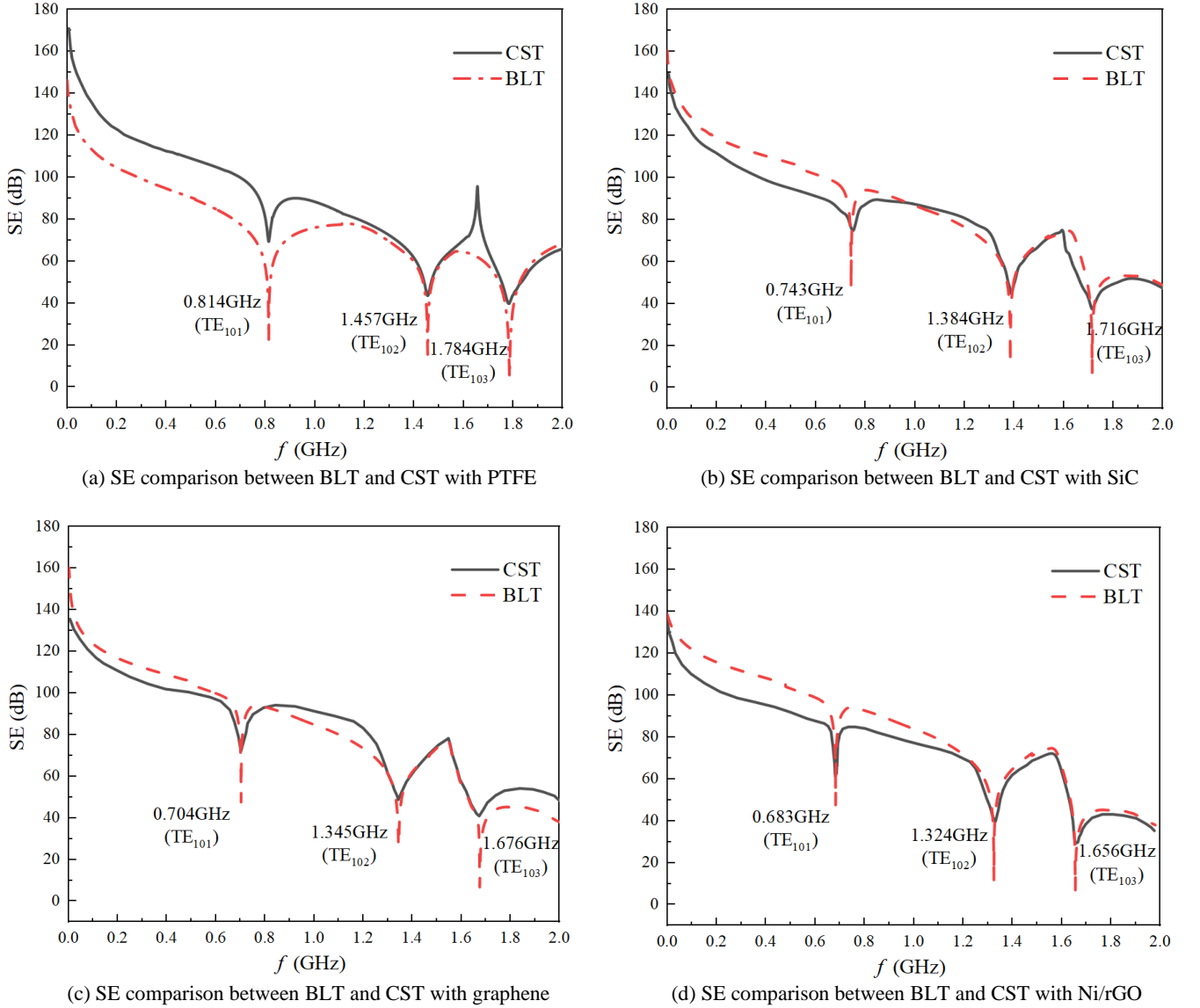(d) SE comparison between BLT and CST with Ni/rGO

Fig. 7. SE comparison in various materials.

From Fig. 7, it can be seen that the BLT equation accurately predicts the resonant frequency of the cavity in TE_{101}, TE_{102}, and TE_{103} modes. In the 0-2 GHz range, all resonant frequencies of the cavity by the BLT equation are consistent with the ones of the CST simulation results.

From Fig. 8, it is evident that SiC, PTFE, graphene, and Ni/rGO exhibit low error (Δ) between BLT and CST at all frequencies except the resonant frequency, i.e., in TE_{101}, TE_{102}, and TE_{103}. This phenomenon arises due to slot resonance, where the slot size of 100 mm equals half the

wavelength of the incident wave at 1 GHz. Additionally, the voltage at the resonant frequency by BLT is relatively higher than that by CST, resulting in a lower SE value.

Leveraging its equivalent circuit model based on the transmission line theory, the BLT equation requires only 2 % CPU utilization and 0.1 min to complete full-frequency band scanning, whereas CST's finite difference method, as a full-wave three-dimensional numerical simulation, demands 73 % CPU resources and 43 min. This efficiency difference is directly reflected in resonant characteristic analysis.

Although both methods yield highly consistent predictions for resonant frequencies, such as TE_{101} and TE_{102}, as shown in Fig. 7, the BLT equation exhibits approximately 8 dB errors in SE calculations at resonant points (as seen in Fig. 8) due to model simplification, and therefore cannot provide a detailed internal field distribution of the cavity. In contrast, despite the longer computation time, CST can precisely quantify SE at resonant points and completely present three-dimensional field distributions, particularly demonstrating an accurate analytical capability for physical mechanisms of higher-order modes, such as TE_{103}, affected by absorbing material thickness.
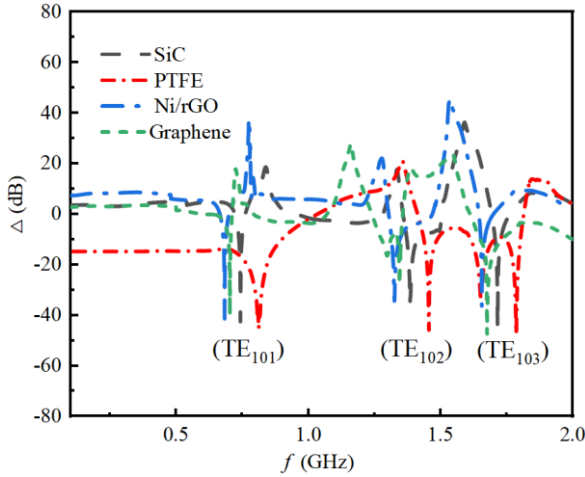

Fig. 8. BLT equations and CST error curves for four materials.

The average error ($\overline{\Delta}$) between BLT and CST in the four materials is summarized in Table 2, not exceeding 8 dB. It verifies the effectiveness of the BLT method in the SE of rectangular cavities coated with absorbing materials on the inner wall.

Table 2. Average error in different materials.

Material	SiC	PTFE	Graphene	Ni/rGO
$\overline{\Delta}$ [dB]	6.01	7.16	6.68	7.33

The comparison of the average CPU utilization rate and the mean calculation time between analysis methods is shown in Table 3. It shows that the proposed model has a significantly lower average CPU utilization rate, i.e., 2 %, compared to CST software, i.e., 73 %. In the mean calculation time, the proposed model takes only 0.1 min, which is much shorter than the 43 min required by the CST software. It reveals that the proposed model can provide both fast and effective analysis in the exploration of the thickness related to the cavity shielding capability.

Table 3. Comparison of average CPU utilization rate and computational time.

Computational method	Average CPU utilization rate [%]	Mean calculation time [min]
The proposed model	2	0.1
CST software	73	43

B. Simulation analysis

The resonant frequency of the cavity with various thicknesses of absorbing materials under resonant modes TE_{101}, TE_{102}, and TE_{103} is explored in this study. According to the electronic industry standard rubber-based wave absorbing plate specification SJ 21488-2018 [25], the thickness of the wave absorbing material was selected as 0.5 mm, 1 mm, 1.5 mm, 2 mm, 2.5 mm, and 3 mm.

The SE comparison in porous cavity coating at 0-2 GHz for four materials is shown in Fig. 9. It is observed that Ni/rGO exhibits the strongest electromagnetic shielding capability, while PTFE has the least effective shielding. It implies that Ni/rGO can convert incident electromagnetic waves into thermal energy more efficiently, allowing it to be dissipated via the dielectric.
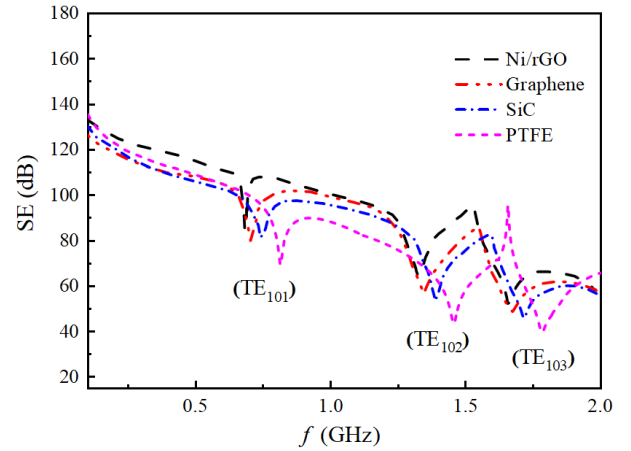

Fig. 9. SE in different absorbing materials.

The effect of coated thickness on various materials, especially in locations with higher resonant frequencies, is shown in Fig. 10. For graphene, it is observed that the resonant frequencies in the TE_{101} and TE_{102} resonant modes correspond to 0.704 GHz and 1.345 GHz, respectively, as shown in Fig. 10(a). However, at the high-order resonant TE_{103}, the resonant frequencies decrease with an increase in the material thickness.

- The 3 mm thickness corresponds to 1.641 GHz,
- the 2.5 mm thickness corresponds to 1.649 GHz,
- the 2 mm thickness corresponds to 1.677 GHz,
- the 1.5 mm thickness corresponds to 1.663 GHz,
- the 1 mm thickness corresponds to 1.661-1 GHz, and
- the 0.5 mm thickness corresponds to 1.667 GHz.

It shows that the change of absorbing material thickness may affect the location of the high resonance. Through equations (10)‑(20), it is revealed that the material thickness can influence the real and imaginary parts of electromagnetic parameters in the complex frequency domain. In practice, the electromagnetic parameters of graphene can be measured using the coaxial method in the frequency range of 1-18 GHz [26]. In reality, due to the weak magnetic properties of graphene materials, the real part of the complex permeability is 1, and the imaginary part is 0. As a result, only the complex dielectric constant is considered here. According to (22), the resonant frequency increases as the complex dielectric constant decreases.

(a) Effect of coated thickness in graphene

(b) Effect of coated thickness in SiC

(c) Effect of coated thickness in PTFE

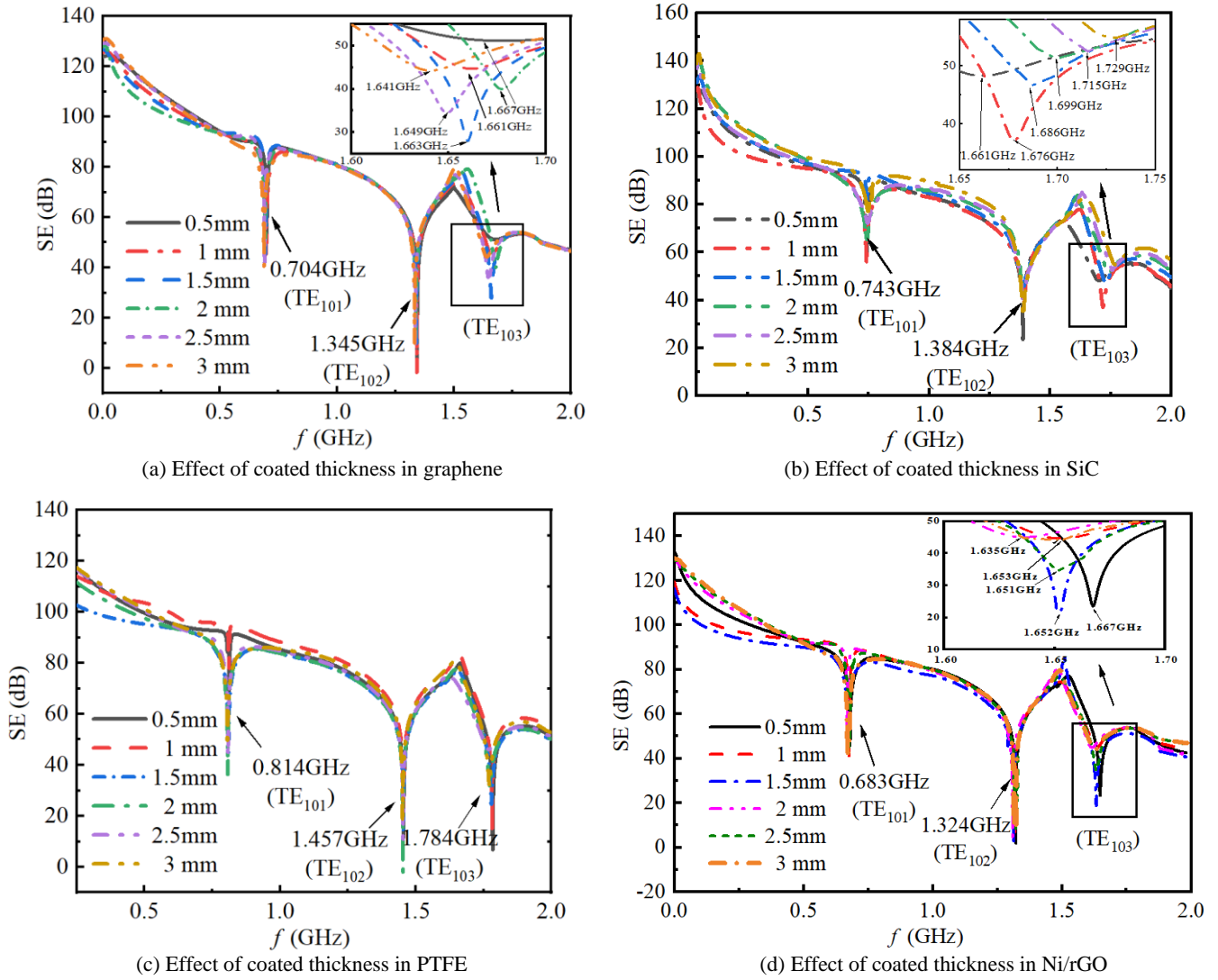(d) Effect of coated thickness in Ni/rGO

Fig. 10. Effect of coated thickness in various materials.

As shown in Fig. 10(b), when the cavity is coated with SiC, the resonant frequencies for modes TE_{101} and TE_{102} are 0.743 GHz and 1.384 GHz, respectively, where the thickness of the coating does not change the resonant frequencies. However, the thickness has a significant influence on the frequency at the resonant mode TE_{103}. For example, a coating of 0.5 mm thickness corresponds to 1.661 GHz, a coating of 1 mm thickness to 1.676 GHz, a coating of 1.5 mm thickness to 1.686 GHz, a coating of 2 mm thickness to 1.699 GHz, a coating of 2.5 mm thickness to 1.715 GHz, and a coating of 3 mm thickness to 1.729 GHz. The real and imaginary parts of the complex permittivity in SiC remain almost unchanged with increasing frequency, while the real part of the complex permeability decreases with increasing frequency [11]. Similar to graphene, the resonant frequency in SiC increases along with a decrease in the complex dielectric constant. Also, it reveals that the material thickness influences the location of higher resonant frequencies.

In Fig. 10(c), resonant frequencies correspond to 0.814 GHz, 1.457 GHz, and 1.784 GHz at modes TE_{101}, TE_{102}, and TE_{103}, respectively, when the cavity is coated with PTFE. It reveals that the coating thickness does not influence

the resonant frequency, while the thickness of PTFE can affect the SE. Indeed, the complex dielectric constant and complex magnetic permeability in PTFE do not vary with frequency. It implies that the thickness of PTFE material may not change the resonant frequency [12].

In Fig. 10(d), when the cavity is coated with Ni/rGO, the thickness has little influence on the resonant frequency in the TE_{101} and TE_{102} modes. However, in mode TE_{103}, the thickness has a significant influence on the resonance at the higher-order frequency. For instance, the coating with a thickness of 0.5 mm corresponds to a resonant frequency of 1.667 GHz, while 1 mm and 3 mm thicknesses correspond to 1.653 GHz, 1.5 mm thickness to 1.652 GHz, 2 mm thickness to 1.635 GHz, and 2.5 mm thickness to 1.651 GHz. Therefore, the change of Ni/rGO thickness can affect the higher-order resonant frequency at TE_{103}. It is noted that the material thickness can affect the real and imaginary parts of electromagnetic parameters. On the other hand, the real and imaginary parts of the complex permittivity in Ni/rGO remain almost unchanged with increasing frequency. However, the real part of the complex permeability decreases with increasing frequency [13].

The SE comparison of absorbent materials with different thicknesses is shown in Fig. 11, indicating the SE related to the coated thickness in all materials. We observe that the cavity shielding performance achieves its best efficacy when the thickness of graphene is 2 mm, with an SE value of 56.98 dB. When the thickness of SiC is 2 mm, the SE is the best with an SE value of 86.84 dB; when the thickness of PTFE material is 1 mm, the SE is the largest with an SE value of 74.95 dB. When the thickness of Ni/rGO is 2 mm, the SE is optimal with an SE value of 52.38 dB.
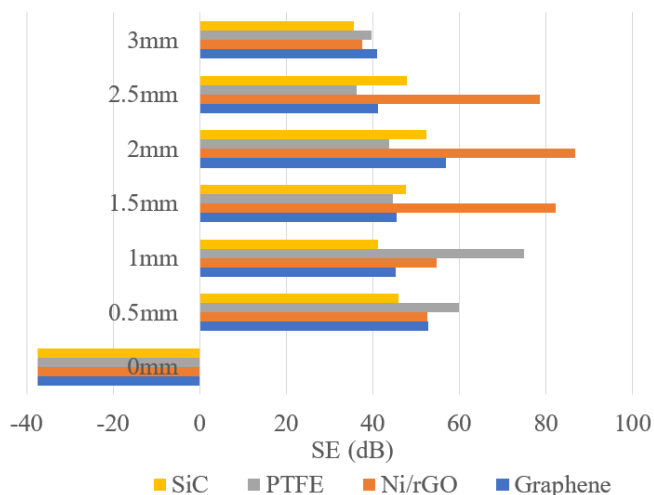

Fig. 11. Comparison of SE with different thicknesses.

5. CONCLUSION

In this study, the BLT-based equation analytical model has been successfully established to accurately calculate the SE of absorbing materials. It verifies that the results obtained using the BLT equation and CST simulation are very close, with an error of less than 8 dB. More importantly, the BLT equation model calculates the SE and resonant frequency more quickly than CST. In conclusion, the BLT equation can rapidly complete single SE calculations, enabling quick optimization of multiple variables, such as material thickness and dielectric parameters. This makes it particularly suitable for preliminary rapid parameter scanning and resonant risk assessment. While CST simulations are more time-consuming, they can accurately capture the field distribution characteristics of higher-order resonant modes, such as TE_{103}, providing critical evidence for understanding electromagnetic energy coupling paths and an effective means for final design validation and mechanism investigation.

It also confirms that the inner wall of the cavity, coated with a graphene, SiC, and Ni/rGO composite material, has no effect on the frequency at the TE_{101} and TE_{102} resonant modes; however, an effect occurs at the higher-order resonant TE_{103} modes. However, the coated thickness using PTFE does not change the resonant frequency of the cavity. Moreover, the 2 mm thickness of the cavity wall coated with graphene, SiC, or Ni/rGO composite materials is found to achieve the best electromagnetic shielding performance. On the other hand, a 1 mm thick coating using PTFE can achieve the best SE in the cavity wall.

REFERENCES

[1] Backstrom, M. G., Lovstrand, K. G. (2004). Susceptibility of electronic systems to high-power microwaves: Summary of test experience. *IEEE Transactions on Electromagnetic Compatibility*, 46 (3), 396-403. https://doi.org/10.1109/TEMC.2004.831814

[2] You, G., Wie, L., Zhou, S. (2020). Electromagnetic protection design and testing and rectification of VPX chassis. *Safety and Electromagnetic Compatibility*, 6, 55-59.

[3] Jongjoo, S., Dong, G. K., Jong, H. K., Joungho, K. (2010). Circuital modeling and measurement of shielding effectiveness against oblique incident plane wave on apertures in multiple sides of rectangular enclosure. *IEEE Transactions on Electromagnetic Compatibility*, 52 (3), 566-577. https://doi.org/10.1109/TEMC.2009.2039483

[4] Gong, Y. F., Hao, J. H., Jiang, L. H. et al. (2018). An analytic model of double-cavity electromagnetic leakage based on Bethe small hole coupling theory and the mirror principle. *Journal of Electrical Technology*, 33 (09), 2139-2147.

[5] Solin, J. R. (2011). Formula for the field excited in a rectangular cavity witha small aperture. *IEEE Transactions on Electromagnetic Compatibility*, 53 (1), 82-90. https://doi.org/10.1109/TEMC.2010.2053711

[6] Zhang, Y., Tian, Z., Wang, C., Yang, Q., Wang, S. (2022). Research on the variation of shielding effectiveness of double-layer shielding enclosure with the position and number of apertures. *Transactions of China Electrotechnical Society*, 37 (13), 3350-3360. https://doi.org/10.19595/j.cnki.1000-6753.tces.210988

[7] Wang, D., Shi, C., Cai, X., Yi, Z. (2019). Research on the shielding effectiveness of rectangular cavitywith embedded thin plate under HEMP irradiation. *Journal of Microwaves*, 35 (1), 87-90. https://doi.org/10.14183/j.cnki.1005-6122.201901017

[8] Kraft, C. H. (1994). Modeling leakage through finite apertures with TLM. In *Proceedings of IEEE Symposium on Electromagnetic Compatibility*. IEEE, 73-76. https://doi.org/10.1109/ISEMC.1994.385681

[9] Hao, J. H, Jiang, L. H, Qian, S. Y. (2020). Efficiency of built-in media plate based on BLT equation. *Journal of Electrical Technology*, 35 (18), 3791-3801.

[10] Dahlang, T., Sultan, I., Bualkar, A., Bidayatul, A., Hee, J. K. (2018). Electronic properties of composite iron (II, III) oxide (Fe3O4) carbonaceous absorber materials by electron spectroscopy. *Journal of Electron Spectroscopy and Related Phenomena*, 229, 47-51. https://doi.org/10.1016/j.elspec.2018.09.008

[11] Hou, Y., Cheng, L., Zhang, Y., Deng, C., Yang, Z., Chen, Q., Wang, P., Zheng, L. (2017). Electrospinning of Fe/SiC hybrid fibers for highly efficient microwave absorption. *ACS Applied Materials & Interfaces*, 9 (8), 7265-7271. https://doi.org/10.1021/acsami.6b15721

[12] Jia, R. F., Yin, B. L., Zhang, G. H. et al. (2022). Development and characteristics of polytetrafluoroethylene electromagnetic shielding composite film. *Journal of Engineering*, 43 (11), 2916-2923.

[13] Wang, Y. W., Wang, Y. P., Chen, M. J. et al. (2020). Preparation and microwave absorption properties of Ni/RGO composites. *Journal of Anhui University of Technology*, 34 (5), 71-75.

[14] Bideskan, M. Z., Forooraghi, K., Atlasbaf, Z. (2021). Method of lines for analysis of plane wave scattering by periodic arrays of magnetically-biased graphene strips. *Scientific Reports*, 11, 7588. https://doi.org/10.1038/s41598-021-86882-z

[15] Li, M., Nian, H. (2024). Perturbation amplitudes design method based on confidence interval evaluation for impedance measurement. *IEEE Transactions on Industrial Electronics*, 71 (10), 12323-12337. https://doi.org/10.1109/TIE.2024.3352148

[16] Jackson, J. D. (1998). *Classical Electrodynamics, 3rd Edition*, Wiley, ISBN 978-0471309321.

[17] Pozar, D. M. (2011). *Microwave Engineering, 4th Edition*. Wiley, ISBN 978-0-470-63155-3.

[18] Andrews, J. R. (2003). UWB signal sources, antennas and propagation. In *2003 IEEE Topical Conference on Wireless Communication Technology*. IEEE. https://doi.org/10.1109/WCT.2003.1321594

[19] Walter, M. W. (2023). Mode matching analysis of waveguide discontinuities. In *IEEE MTT-S International Symposium*. IEEE.

[20] Yan, F., Liu, X. H., Wang, P. et al. (2019). Shielding effectiveness of metallic cavities with different aperture arrays in high intensity radiated field. *Electronics Optics and Control*, 26 (8), 90-94.

[21] Ramo, S., Whinnery, J. R., Van Duzer, T. (1994). *Fields and Waves in Communication Electronics, 3rd Edition*. Wiley, ISBN 978-0-471-58551-0.

[22] Hy, J. (2023). *Preparation of dielectric/magnetic loss doped graphene aerogel and its microwave absorbing properties*. Thesis, Zhengzhou Institute of Aeronautical Industry Management, Zhengzhou, China.

[23] Tan, H. B. (2011). The electromagnetic shielding effectiveness of SiC with cobalt coating by electroless plating. *Shandong Ceramics*, 34 (1), 14-16.

[24] Gao, X., Su, J., Liu, H., Zhang, L., Chen, M. (2016). Design and electromagnetic performance analysis of new absorbing materials. *Chinese Journal of Power Sources*, 40 (7), 1467-1468+1500.

[25] China Electronics Standardization Institute. (2018). *Specification for rubber-based wave absorbing plate*. SJ 21488-2018.

[26] Liu, W., Xiong, J., He, S., Luo, G., Xia, L., Lan, X. (2022). Ultra wideband graphene foam absorbing materials with multilayer structure design. *Journal of Ordnance Equipment Engineering*, 43 (2), 197-203.